



## Article

# Fluorine-18 Fluorodeoxyglucose Isolation Using Graphene Oxide for Alternative Radiopharmaceutical Spillage Decontamination in PET Scan

Mohammad Khairul Azhar Abdul Razab <sup>1,\*</sup> , Norazlina Mat Nawi <sup>2,\*</sup>, Fara Hana Mohd Hadzuan <sup>1</sup>, Nor Hakim Abdullah <sup>3</sup>, Maimanah Muhamad <sup>4</sup>, Rosidah Sunaiwi <sup>1</sup>, Fathirah Ibrahim <sup>1</sup>, Farah Amanina Mohd Zin <sup>3</sup>  and An'amt Mohamed Noor <sup>3</sup>

- <sup>1</sup> Medical Radiation Programme, School of Health Sciences, Universiti Sains Malaysia, Health Campus, Kubang Kerian 16150, Kelantan, Malaysia; farahadzuan@student.usm.my (F.H.M.H.); rosidah98@student.usm.my (R.S.); fathirah\_ibrahim94@yahoo.com (F.I.)
  - <sup>2</sup> Department of Nuclear Medicine, Radiotherapy & Oncology, School of Medical Sciences, Universiti Sains Malaysia, Health Campus, Kubang Kerian 16150, Kelantan, Malaysia
  - <sup>3</sup> Advanced Materials Research Cluster, Faculty of Bioengineering and Technology, Universiti Malaysia Kelantan, Jeli Campus, Jeli 17600, Kelantan, Malaysia; norhakimin@umk.edu.my (N.H.A.); farahamanina2751@gmail.com (F.A.M.Z.); anamt@umk.edu.my (A.M.N.)
  - <sup>4</sup> Nuclear Medicine & Molecular Imaging Department, Chancellor Tuanku Muhriz Hospital, Universiti Kebangsaan Malaysia, Jalan Yaacob Latif, Bandar Tun Razak, Cheras 56000, Kuala Lumpur, Malaysia; maimanah@ppukm.ukm.edu.my
- \* Correspondence: khairul.azhar@usm.my (M.K.A.A.R.); norazlina@usm.my (N.M.N.)



**Citation:** Razab, M.K.A.A.; Nawi, N.M.; Hadzuan, F.H.M.; Abdullah, N.H.; Muhamad, M.; Sunaiwi, R.; Ibrahim, F.; Zin, F.A.M.; Noor, A.M. Fluorine-18 Fluorodeoxyglucose Isolation Using Graphene Oxide for Alternative Radiopharmaceutical Spillage Decontamination in PET Scan. *Sustainability* **2022**, *14*, 4492. <https://doi.org/10.3390/su14084492>

Academic Editors: Hosam M. Saleh and Mohammad Mahmoud Dawoud

Received: 16 March 2022

Accepted: 7 April 2022

Published: 9 April 2022

**Publisher's Note:** MDPI stays neutral with regard to jurisdictional claims in published maps and institutional affiliations.



**Copyright:** © 2022 by the authors. Licensee MDPI, Basel, Switzerland. This article is an open access article distributed under the terms and conditions of the Creative Commons Attribution (CC BY) license (<https://creativecommons.org/licenses/by/4.0/>).

**Abstract:** Radiopharmaceuticals (RPC) used for diagnostic and therapeutic purposes in nuclear medicine may contaminate surface areas due to spillage during its preparation or accident during RPC transfer from laboratory to the treatment room. Fluorine-18 Fluorodeoxyglucose (<sup>18</sup>F-FDG) is the most common RPC for positron emission tomography (PET) scan in nuclear medicine due to its ideal annihilation converted energy at 511 keV and short half-life at 109.8 min. Ineffective medical waste management of <sup>18</sup>F-FDG may pose a risk to the environment or cause unnecessary radiation doses to the personnel and public. Depending on the incident rate of these events, simple decontamination methods such as the use of chemicals and swabs might not be cost-effective and sustainable in the environment. This study aims to propose an alternative method to decontaminate <sup>18</sup>F-FDG by using graphene oxide (GO). GO was synthesised using the Hummers method while the physical morphology was analysed using a field emission scanning electron microscope (FESEM). <sup>18</sup>F-FDG adsorption efficiency rate using GO nanolayers was analysed based on the kinetic study of the GO:<sup>18</sup>F-FDG mixtures. The chemical adsorbability of the material was analysed via UV–vis spectrophotometer to interlink the microstructures of GO with the sorption affinity interaction. Resultantly, the adsorption rate was effective at a slow decay rate and the optical adsorption of GO with <sup>18</sup>F-FDG was dominated by the  $\pi \rightarrow \pi^*$  plasmon peak, which was near 230 nm. By elucidating the underlining GO special features, an alternative technique to isolate <sup>18</sup>F-FDG for the decontamination process was successfully proven.

**Keywords:** radiopharmaceutical; radioactive spillage; decontamination; radioactivity; adsorption; nuclear medicine

## 1. Introduction

Radiopharmaceutical (RPC) resources are essential for nuclear imaging and therapeutic purposes in nuclear medicine. Fluorine-18 Fluorodeoxyglucose (<sup>18</sup>F-FDG) is the most ideal RPC for positron emission tomography (PET) scans due to its ideal half-life and versatile molecular structure [1,2]. Fluorine is considered a favourable atom in drug development due to its physical properties, including a small van der Waals radius (1.47 Å),

high electronegativity, and ability to form a strong bond with carbon (C-F energy bond of 112 kcal/mol) [3]. In comparison with a carbon-hydrogen bond (C-H energy bond of 98 kcal/mol),  $^{18}\text{F}$ -FDG is more thermally stable and oxidation resistant [3]. Unexpected radioactive contamination might occur in a nuclear medicine department either from source handling, such as breakage of a radionuclide vial, or may originate from the patient either by sneezing, vomiting, or urinating [4]. The hazard associated with radioactive contamination and waste depends on the concentration and nature of the activity of the radionuclide [5].  $^{18}\text{F}$ -FDG, an unstable radioisotope, will decay in the human metabolic process and produce positrons, thereby leading to an annihilation process with electrons and producing pairs of 511 keV gamma-ray photons in 180° directions [6]. This energy is quite high and exposes the personnel, patient, and public to unnecessary radiation doses.

The high demand for PET scans requires mass production of  $^{18}\text{F}$ -FDG using cyclotron, which indirectly leads to an increase in the incident rate of radionuclide spillage contaminations. Meanwhile, the usage of a large volume of simple decontamination chemical agents might not be sustainable in the environment [7], and is not cost-effective as its periodic purchase is met with limited production. Thus, alternative decontamination agents must be considered by ensuring the application of a competent material for radionuclide decontamination, which is more efficient, environmentally friendly, and economical in terms of long-term usage of the resources [8].

Graphene oxide (GO) is a nanolayer material that has a carbon compound and is rich in oxygenated functional groups, which makes it a fitting adsorbent for various molecules either in aqueous or dispersed in a polymeric solution [9]. GO also has several desirable properties, such as high surface area, high mechanical strength, electrical conductivity, large pore volume structure, and high solubility due to abundant oxygen-based functional groups [9]. GO is a two-dimensional (2D), carbon-based material that has a single-atom-thin full  $\text{sp}^2$  hybridised carbon structure with minimal defects, which makes it a well-known adsorbent [10]. Due to its uniquely tuneable physicochemical characteristics [11] and biocompatibility [12], GO has been used in many applications such as the removal of metal ions [13], biomedical [14], electrochemical energy [15], catalysis [16], sensing [17], polymers composite [18], removal of heavy metals [19], wastewater treatment [20] and antibacterial agents [21].

The availability of various functional groups such as carboxyl, hydroxyl, epoxy and keto groups on its nano surface [22] give advantages to GO as a super adsorbent carbon material to efficiently interact with any hazardous and toxic liquid, gas or solid contaminants [23]. Practically, radioactive waste has been decontaminated using special chemical agents which might chemically produce other chemical by-products [24] due to chemical interactions with unstable energetic radionuclide.

Application of GO nanosheets in trapping radionuclides has been conducted on  $^{238}\text{U}$  [25],  $^{137}\text{Cs}$  [26],  $^{131}\text{I}$  [27],  $^{232}\text{Th}$ ,  $^{95}\text{Am}$ ,  $^{94}\text{Pu}$ ,  $^{63}\text{Eu}$ ,  $^{38}\text{Sr}$  and  $^{99\text{m}}\text{Tc}$  [28]. However, adsorption and chemical adsorption characterization of short-live radionuclides such as the  $^{18}\text{F}$  radionuclide by using GO has not been comprehensively reported. Herewith, we conduct experiments to prove the efficiency of  $^{18}\text{F}$ -FDG decontamination by using GO, which is a stable carbon-based material with minimal production of chemical by-products. The interactions between these compound mixtures with different concentration of GO and activities for energy variations were characterized by using UV-vis spectrometer for complex adsorption capabilities.

## 2. Materials and Methods

Graphite powder, a naturally occurring form of crystalline carbon along with inorganic compound potassium permanganate ( $\text{KMnO}_4$ ) and corrosive substances, sulphuric acid ( $\text{H}_2\text{SO}_4$ ) and phosphoric acid ( $\text{H}_3\text{PO}_4$ ), were used to make up the GO mixture. Hydrogen peroxide ( $\text{H}_2\text{O}_2$ , 30%) and ice cubes were used to initiate and phase out the oxidation process. Consequently, hydrochloric acid ( $\text{HCl}$ ) and distilled water were used for the centrifuge process.  $^{18}\text{F}$ -FDG was obtained at the Nuclear Medicine & Molecular Imaging

Department, Chancellor Tuanku Muhriz Hospital, Universiti Kebangsaan Malaysia. A dose calibrator (Capintec CRC-25R, Capintec Inc., Florham Park, NJ, USA) was used to monitor and record the activity of the radionuclides. The characterisation of the synthesised GO was performed using FESEM (FEI QuantaTM 450 FEG, FEI Company, Hillsboro, OR, USA) at SEM Laboratory, School of Health Sciences, Universiti Sains Malaysia. Furthermore, a morphological analysis of the nanolayers and their porosity was conducted. Meanwhile, the chemical adsorbability affinity of the GO- $^{18}\text{F}$ -FDG was analysed using a UV-vis spectrometer (CARY 100 Bio, Agilent Technologies Inc., Santa Clara, CA, USA) at the Analytical Laboratory, School of Health Sciences, Universiti Sains Malaysia.

### 2.1. Synthesis of Graphene Oxide

The Graphene oxide was synthesised by the widely used Hummer's method [29–31]. About 3 g of graphite and 18 g of  $\text{KMnO}_4$  were added to the 320 mL of  $\text{H}_2\text{SO}_4$  and 80 mL of  $\text{H}_3\text{PO}_4$  in a ratio of 4:1, respectively. The mouth of the beaker was closed with an aluminium foil and stirred for three days continuously before transferring the reagent into a 500 mL ice cube along with 27 mL of  $\text{H}_2\text{O}_2$  (30%) to stop the oxidation and cooling process. The dark brown mixture formed was known as graphite oxide, which was then washed with HCl to separate the GO from the chemical by-products and unexfoliated graphite. About 15 mL of the mixture and 15 mL of HCL were mixed and centrifuged at 5000 g/rpm for 10 min. This washing process was repeated thrice before washing with distilled water several times and centrifuged with the same setting until a pH of 5 was achieved.

### 2.2. Isolation of $^{18}\text{F}$ -FDG

The GO concentrations were varied into 1 mg/mL, 2 mg/mL, and 3 mg/mL, which were obtained by applying Equation (1), where  $M_1$  is the initial concentration of the solution,  $V_1$  is the volume of the solution,  $M_2$  is the concentration of the diluted solution after adding more solvent, and  $V_2$  is the volume of the diluted solution.

$$M_1 V_1 = M_2 V_2 \quad (1)$$

The FDG dispenser (NUCLEMED 317R3, NUCLEMED BV, Roeselare, Belgium) was used to accurately prepare the 37 MBq, 74 MBq, and 111 MBq of  $^{18}\text{F}$ -FDG, and three different concentrations of GO were added into each glass serum vial as shown in Figure 1a. The mixture of GO- $^{18}\text{F}$ -FDG was then poured on a filter paper, and the sediment was obtained as depicted in Figure 1b. The radioactivity of the sediment along with the filter paper and the filtrate (if available) were obtained using the dose calibrator ionisation chamber over the function of time ( $A_0$  = initial activity,  $A_0/4$  = 54.9 min,  $A_0/2$  = 109.8 min,  $A_0/3$  = 164.7 min, and  $A_0/16$  = 219.6 min). The radioactivity of each activity with different concentrations was compared to the natural decay of  $^{18}\text{F}$ -FDG by plotting the decay graph. A Geiger-Muller survey meter (Model Fluke 451B, Fluke Corporation, Everett, WA, USA) was used during the experiment to measure the radiation exposure, ensuring there was no leakage or spillage of the radionuclide source on any surfaces in the laboratory.

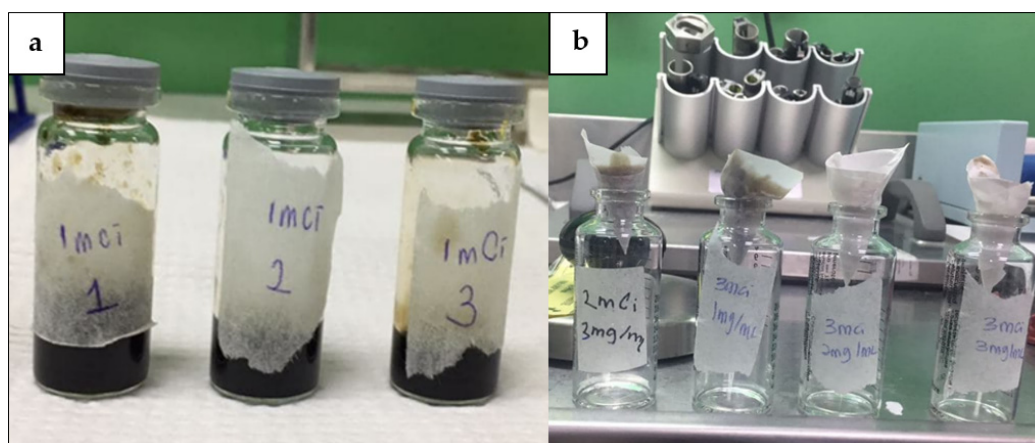


**Figure 1.** (a) GO solution with 1 mg/mL, 2 mg/mL and 3 mg/mL mixed with  $^{18}\text{F}$ -FDG of 1mCi ( $\sim 37$  MBq) in glass serum vials. (b) GO: $^{18}\text{F}$ -FDG mixture poured into filter papers.

### 3. Results and Discussions

#### 3.1. Characterisation of GO Nanolayers

Graphene oxide (GO) images obtained from the FESEM were well defined and interlinked two-dimensional (2D) graphene sheets. Figure 2a,b show random sophisticated 2D structures with different magnifications. The surface appears as a wrinkly ‘wax tissue layer’ with hollow structures (red arrows in Figure 2a) and a continuous vast layer-by-layer surface area with random size of GO flakes (numbering layers in Figure 2b). This feature is advantageous to the GO in terms of ‘wrapping’ or entrapping other materials with various chemical bonds by the numerous carbon functional groups existing at the molecular structure level [32]. It also shows that the ‘wax tissue layer’ [33,34], which resembles the GO sheet, reflects that the deformation of the graphene layers was due to the oxidation process in the synthesised GO. Hence, the carbon lattice became distorted following the addition of oxygen lattice into the structures [35]. The generated hollow pores as shown in Figure 2a could be formed via the hydrothermal method by crumpling graphene sheets together, which results in the formation of voids between the sheets [32]. These features in the GO appear to be advantageous in terms of the hydrophilicity and dispersion into various media, including aqueous and organic solvents.

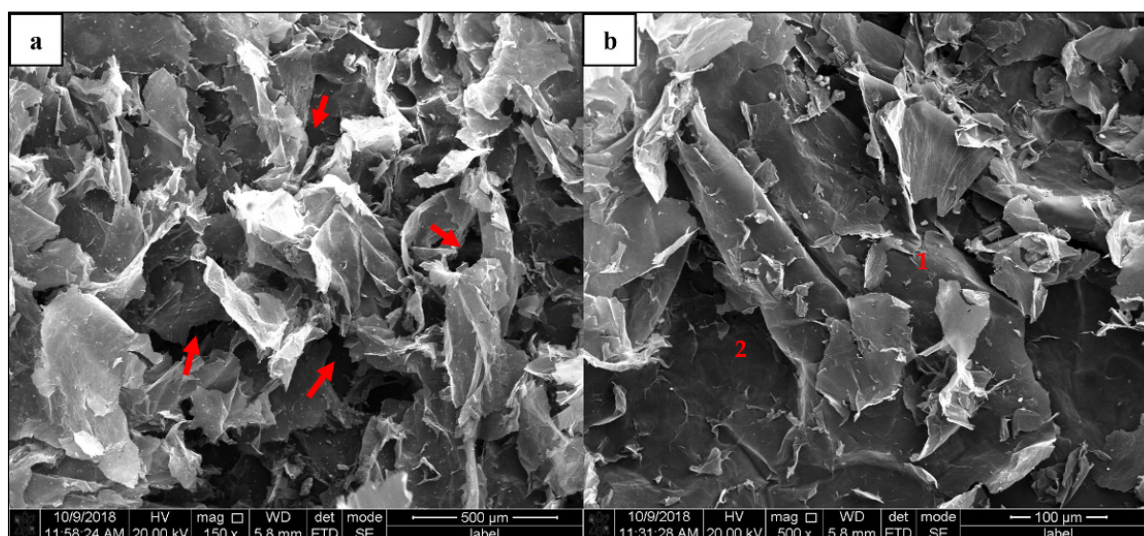


**Figure 2.** GO flake 2D structures with random ‘wax-tissue’ layers and complex hollow structures. (a) Complex hollow structures with wrinkles and exfoliated tissue layers, (b) wrinkles and exfoliated stacked structures with random small flakes.



Stacked GO structures can be clearly seen in Figure 3a,b for 250 $\times$ , and 500 $\times$  magnification. The stacking structures enhance the continuous interaction probabilities with other compounds, where the large substrate surface area will participate in the molecular interactions [33]. The interactions probabilities are continuously increased with stacking layers by layers of GO and might be trapped within the compound with increasing depth via complex interactions.

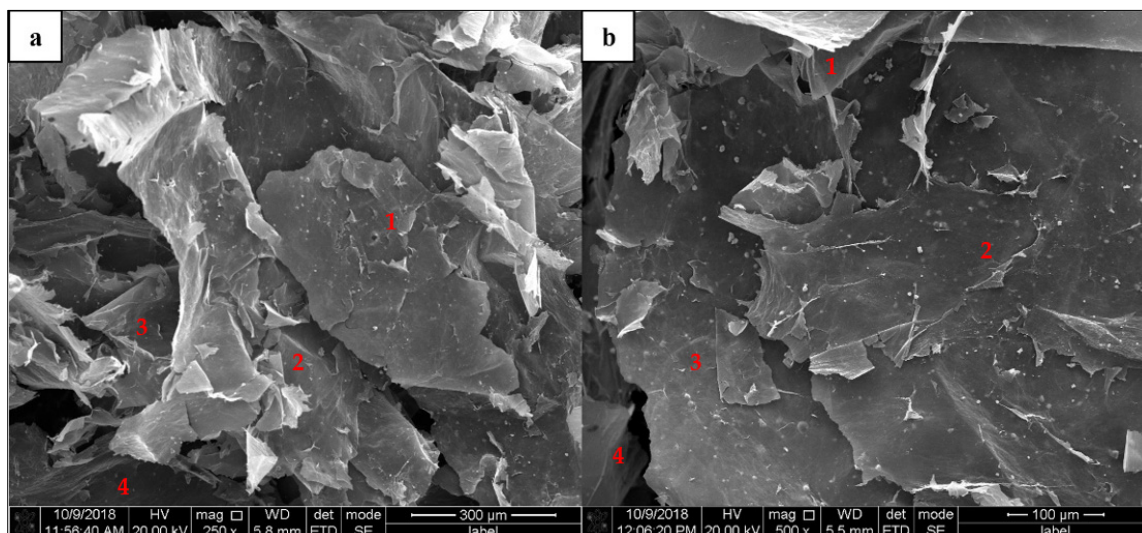


**Figure 3.** GO substrate surface stacked nanostructures. (a) Random stacks of small-flake GO nano-layers, (b) flat surface of large-flake GO nano-layers.

Meanwhile, a single substrate of GO nanolayers can be seen in a close-up micrograph in Figure 4a,b. The micrograph enhances the size of the nano substrate surface for molecular interactions to trap the  $^{18}\text{F}$ -FDG and other compounds. Some contaminants on the GO surface can be seen in Figure 4a, which might be due to the incomplete washing of some foreign particles (red arrows). However, Figure 4b shows a significant structure of single wax tissue layers of GO with wrinkles and exfoliated networking lines on the surface (arrows), ready for the adsorption process via the molecular interaction of many available functional groups.

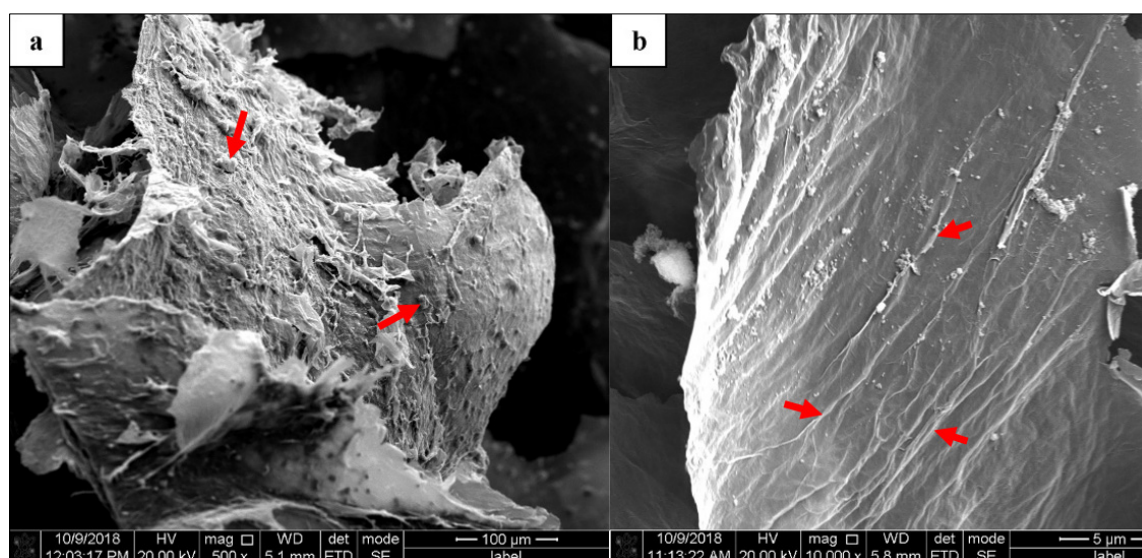


**Figure 4.** Close-up of single substrate GO nanolayers. (a) Contaminants existed on the GO nano-layers, (b) continuous wrinkle and exfoliated networking lines ready for adsorption interactions.

In additions, the complex structures of GO nanolayers have been focused within smaller scales as those shown in Figure 5a,b. The agglomerated ‘wax tissue’ nanolayers with non-uniform structures are shown in Figure 5a. The complex wrinkles and exfoliated structures can be seen via the red arrows, whereas the agglomerated long strand ‘wax-tissue’ nanolayers can be seen on another site. On the other hand, Figure 5b shows the multiple stacking layers that can still be identified from the agglomerated wax tissue layers. These structures demonstrate that the continuous multiplex nanolayers randomly existed for fine focused micrograph and widely spread on the GO substrates.

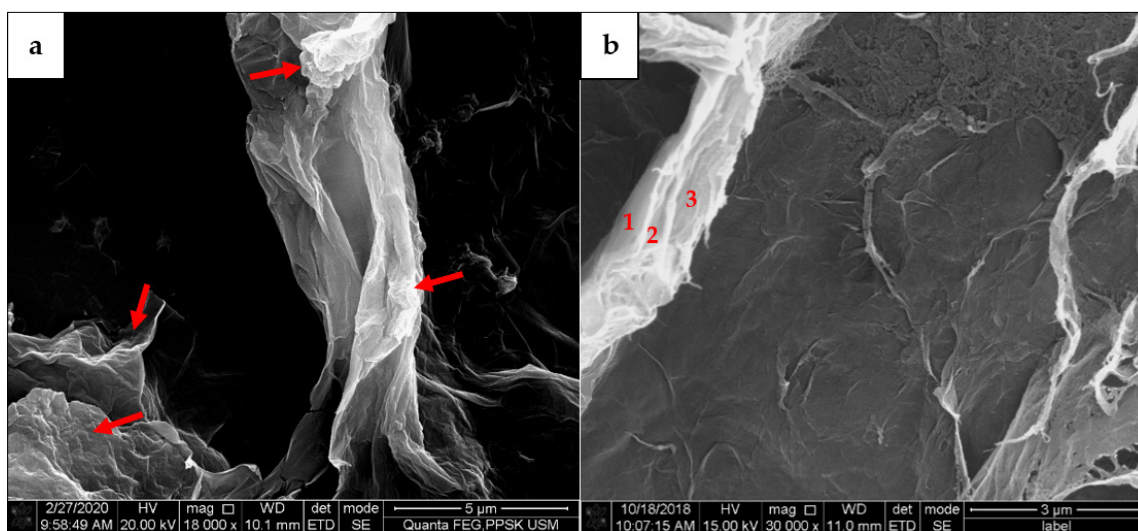


**Figure 5.** Agglomerated ‘wax-tissues’ GO with stacking layers. (a) Random and long strand agglomerated ‘wax-tissue’ nanolayers, (b) identification of stacking layers on agglomerated GO structures.

Moreover, agglomerated wrinkle and exfoliated structures have been further characterized with smaller scales to show a close up image of the 2D single nanolayers of the ‘wax-tissue’ GO structures as shown in Figure 6a,b. It can be seen that the small spherical agglomerated GO nanostructures are randomly attached on the upper site as shown in Figure 6a and the lower site as shown in Figure 6b of the single nanolayers. This phenomenon proves the complex random structures of agglomerated GO nanolayers existed along the stacking surfaces and promote high interactions with any materials via molecular interactions [36]. However, agglomerated unattached spherical nano structures are also randomly seen in Figure 6a, which leads to random complex interactions efficiency during the adsorption process [37].

In Figure 7a, a stacking wrinkles and exfoliated GO nanolayers has been selected for characterization by using X-ray diffraction technique (XRD) (Bruker D2, Bruker Corporation, Billerica, MA, USA) and UV-vis spectrometer. XRD spectrum of the GO is similar to the GO reported in other previous published works. It can be seen in Figure 7b that the characteristic peak of GO centred at  $10.0^\circ$ , which was assigned to the (0,0,1) reflection of GO. The UV-visible adsorption spectra of GO are shown in the Figure 7c. As revealed by the spectrum, two characteristic peaks of GO were observed at 227 and 229 nm, which were  $\pi \rightarrow \pi^*$  transition of aromatic C-C bond and the  $n \rightarrow \pi^*$  of C=O group, respectively. This is in agreement with the results published elsewhere [38].

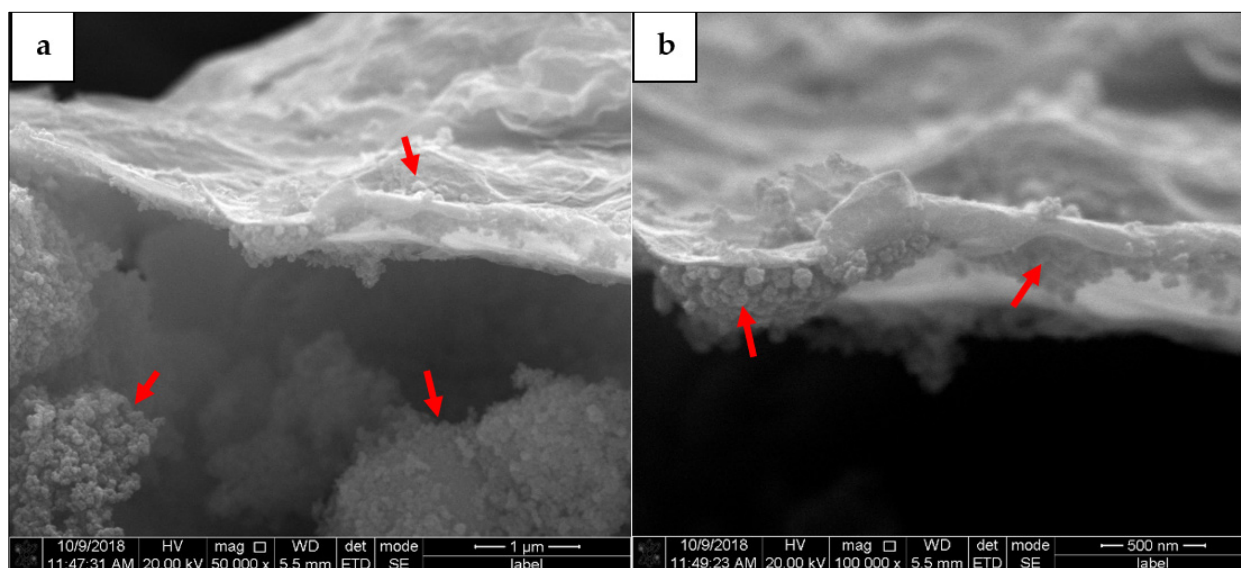


**Figure 6.** (a) Attached and free spherical agglomerated GO structures and (b) small spherical agglomerated GO nano structures have been randomly attached on the stacked wrinkles and exfoliated single GO nanolayer.

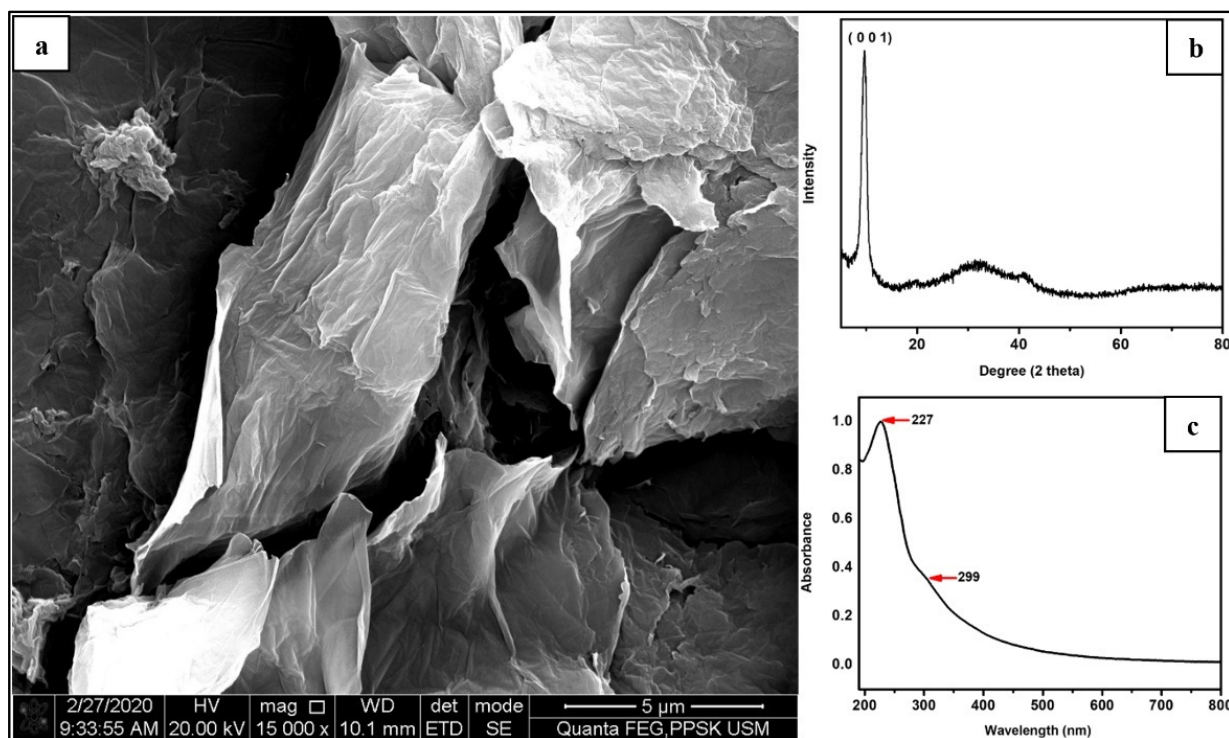


**Figure 7.** (a) Stacking wrinkles and exfoliated GO nanolayers [34], (b) XRD characterization of GO centred at  $10.0^\circ$ , and (c) UV–vis spectrum characteristic peaks of GO observed at 227 and 229 nm.

### 3.2. Kinetic Study

The kinetic study of the isolation of GO: $^{18}\text{F}$ -FDG mixtures for different concentrations of GO concentrations and RPC activities was extrapolated using the radioactive decay equation as shown in Equation (2), where  $A$  is the radionuclide activity,  $A_0$  is the initial radionuclide activity,  $\lambda$  is the decay constant, and  $t$  is the decay time. Each of the activities (37 MBq, 74 MBq and 111 MBq) that were mixed with different GO concentrations (1, 2, 3 mg/mL) and trapped by using a filter paper were measured using a dose calibrator within specific periods (54.9 min,



109.8 min, 164.7 min, and 219.6 min). The activities were differentiated in order to investigate the influence of the positrons and gamma-ray photons' production rate on the molecular adsorption process. Three graphs to study the kinetics of the  $^{18}\text{F}$ -FDG isolated by GO based on activity over time were plotted for different values of  $A_0$  as shown in Figures 8–10.

$$\ln (A/A_0) = -\lambda t \quad (2)$$

Figures 8–10 depict the exponentially plotted graph of GO: $^{18}\text{F}$ -FDG activities versus time for three different concentrations (1, 2, and 3 mg/ mL). From these graphs, the activity of GO: $^{18}\text{F}$ -FDG was exponentially decreased to half from their approximate initial activities within 109.8 min, which is the natural half-life of  $^{18}\text{F}$  [39]. From the graph, the first term half-life for three different activities (37 MBq, 74 MBq and 111 MBq) are sharply reduced due to their active decay processes with respect to its initial activities (high activity), becoming stagnant for the second term of its half-life and approximately close to zero for total decay (219.6 min). The decay process depends on the activities of the radionuclide, where higher activities promote active interactions with random decay processes in the nucleus. In this study, the existence of different concentrations of GO with RPC influenced the nuclear decay process within the unstable  $^{18}\text{F}$  nucleus, where there are different activities has been measured for different concentrations in a specific natural half-life. This phenomenon might be due to the adsorption of GO at the molecular level which is mostly via van der Waals and ionic interactions [40], causing some inter-molecular changes of weak nuclear and electromagnetic forces in  $^{18}\text{F}$  during its decay process. Influence of the weak nuclear forces that control the nuclear activities for any radioisotope decay [41], might cause some changes in the decay rate of the materials during complex molecular interactions.

Generally, 1 mg/mL concentration of GO can trap the  $^{18}\text{F}$ -FDG effectively, where the activity is always higher in each measured time as shown in Figures 8–10. This might be due to random nuclear interaction activities in the  $^{18}\text{F}$  nucleus, where vast numbers of electrons for higher concentrations might fluctuate or slow the molecular interactions. Fluctuation at the initial activity due to a high decay rate may be attributed to the reactivity of the orbital electrons of fluorine, which actively tend to be stabilised via complex interaction [42].

The adsorption interactions might also be influenced by the physical volume of the RPC that coagulate with certain GO concentrations, where the insoluble process might occur due to saturated solutions. It also shows that a higher concentration of GO could reduce the activity of  $^{18}\text{F}$ -FDG due to the interactions occurring at molecular levels. High activities of  $^{18}\text{F}$ -FDG (111 MBq and 74 MBq) actively produce positron, which originates from the nucleus and leads to an annihilation process rather than adsorption interaction with the GO. Figures 9 and 10 show the undifferentiation for low and high concentrations of GO and their influence on the activity decay of  $^{18}\text{F}$ -FDG, where the line is almost redundant with each other. However, the slower decay process provides a likelihood for adsorption interactions, where the line is seen to be identical at 50 min onwards in Figure 6, as well as the whole measurable activity in Figure 8. This might be due to the availability of free electron clouds in  $^{18}\text{F}$ -FDG, which have more chance to be interacted with and form functional groups in the GO chemical structures at low activity.



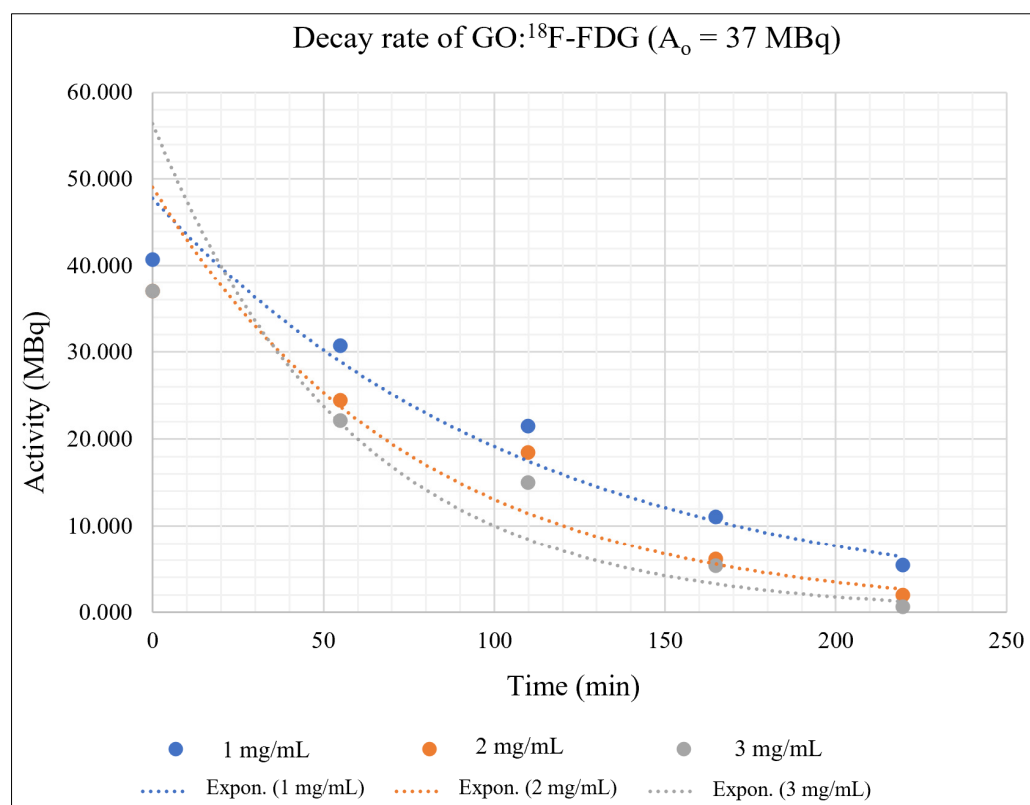


**Figure 8.** GO:<sup>18</sup>F-FDG mixtures with an initial activity of 37 MBq and different concentrations of GO.

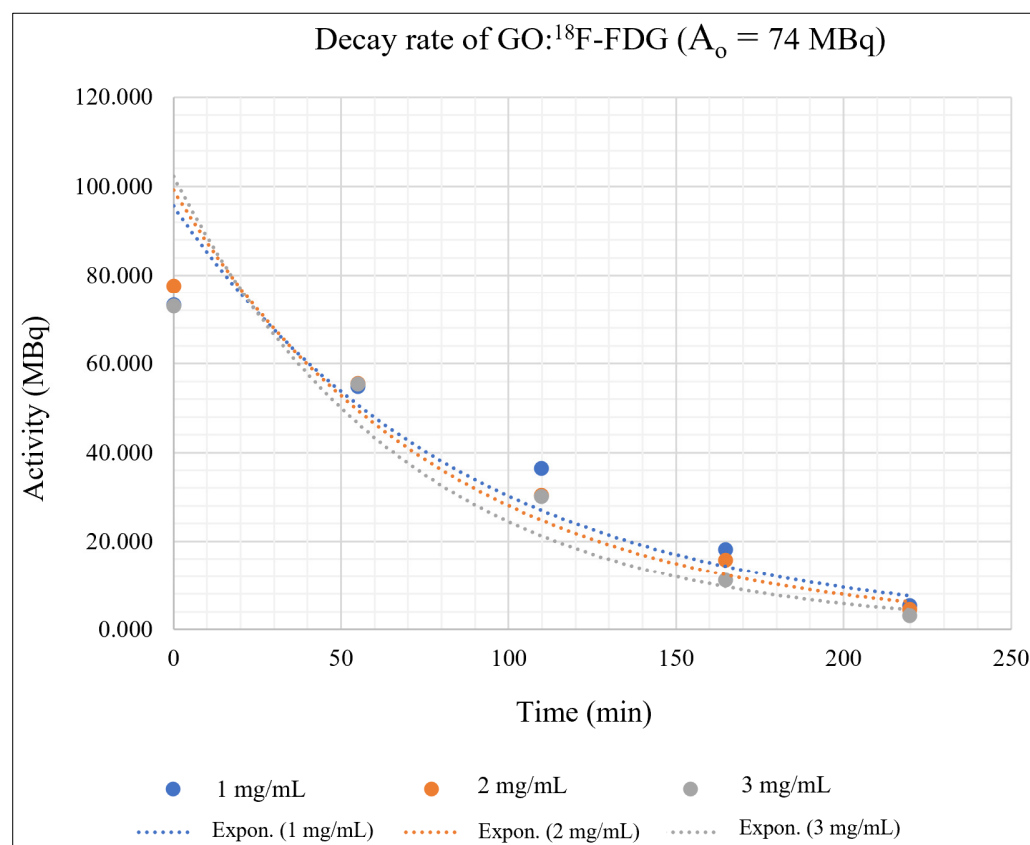


**Figure 9.** GO:<sup>18</sup>F-FDG mixtures with an initial activity of 74 MBq and different concentrations of GO.

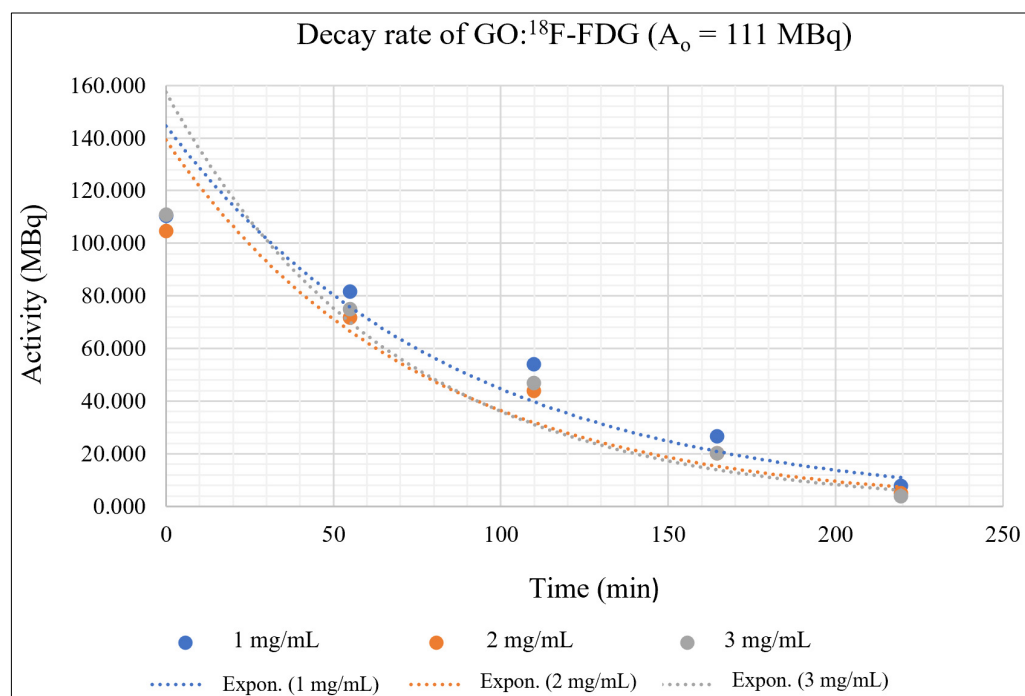


**Figure 10.** GO: $^{18}\text{F}$ -FDG mixtures with an initial activity of 111 MBq and different concentrations of GO.

### 3.3. UV-Vis Spectrometry and Chemical Analysis

The study of absorbability of the graphene oxide and the radionuclide using the UV-vis spectrophotometer provided detailed information about the peak of the wavelength based on the Beer-Lambert law [43]. The GO and  $^{18}\text{F}$ -FDG UV-visible adsorption spectra were obtained as shown in Figure 11. A single band GO adsorption peak can be observed, which was centred at 220 nm as depicted by the dashed red line. This band value indicates the  $\pi \rightarrow \pi^*$ , the transition of aromatic C-C bonds, which have numerous  $\text{sp}^2$  bonds into the molecular mixtures [44]. The molecule absorbs the UV-vis light starting at the wavelength of 200 nm and begins to decline before attaining the peak at 220 nm. Thereafter, the molecule continues to decline to show that the functional group of GO has partially decreased as it passes a higher value of wavelength. The optical adsorption of GO is dominated by the  $\pi \rightarrow \pi^*$  plasmon peak, which is near 230 nm [45]. This occurrence depends on two conjugative effects: clusters of nanometer-scale  $\text{sp}^2$  and the chromophore unit, such as C=C, C=O and C-O bonds [45].

The chemical structure of  $^{18}\text{F}$  is  $1\text{s}^2 2\text{s}^2 2\text{p}^5$  and has a single free orbital electron. It is able to produce high energetic photons with 511 keV which activate the orbital electrons of the functional groups and delocalize on to the GO nano sheets via continuous  $\pi \rightarrow \pi^*$  stacking interactions due to the stacked nanolayers of GO structures. The 511 keV photons energy might eject the orbital electrons at available functional groups to provide free molecular vacancy to be filled in by unstable  $^{18}\text{F}$  atoms. The electrons might interact with epoxy bridges, hydroxyl groups, and pairwise carboxyl groups in GO nanolayers [45] and might be influenced by excess energies received during the internal nuclear decay, leading to the annihilation process as shown in Figure 12.

The peak obtained at 220 nm was probably due to the aggregation of chromophore effects that were affected by the mixture of GO: $^{18}\text{F}$ -FDG for different GO concentrations [46]. The 1 mg/mL showed the highest peak and the highest adsorbability compared to 2 mg/mL and 3 mg/mL of GO concentrations. This result is in line with the kinetic study illustrated in Figure 8, where a slow decay rate of low  $^{18}\text{F}$ -FDG activity provided the chances for the molecular adsorption rate to occur. Higher concentrations might yield a complex saturated phase between the molecular mixtures to interact within a short time, whereas higher activities will generate excess energy to the particles for the annihilation process or eject the electrons from orbitals without interactions. The mixture probably modified the

oxygen-containing functional groups, thereby causing the mixture to absorb a slightly lower range of UV–vis wavelength. The wavelength of adsorption also depends on the energy difference between the bonding or antibonding and non-bonding orbital concerned [47].

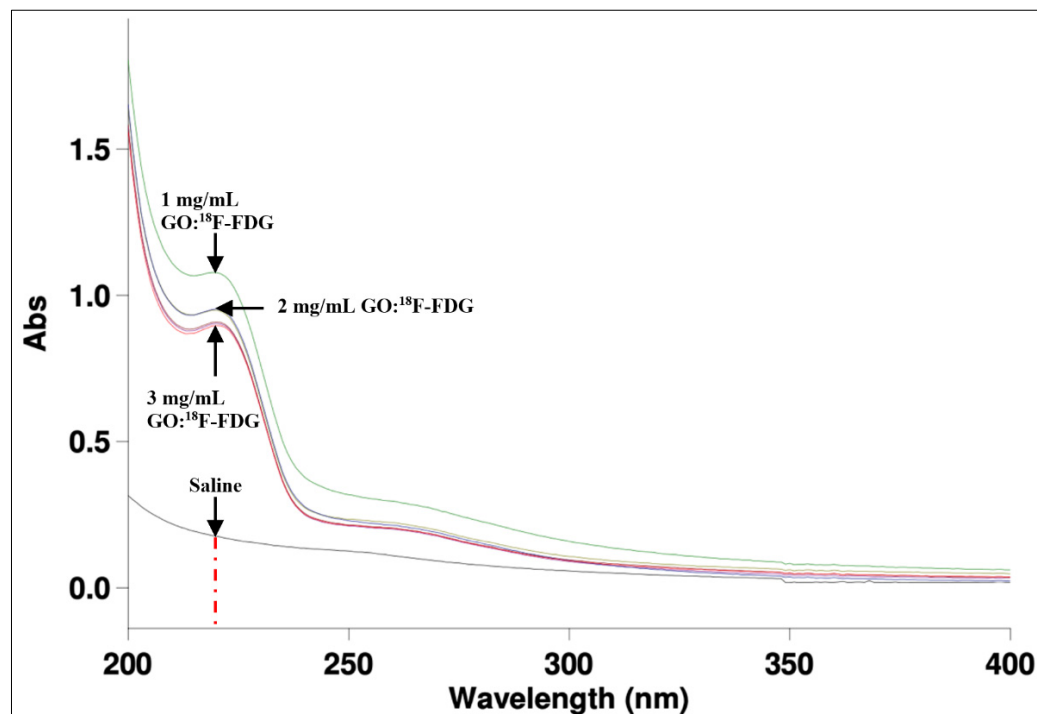


**Figure 11.** The UV–vis adsorption of GO- $^{18}\text{F}$ -FDG with different concentrations has been seen on at the peak of 220 nm.

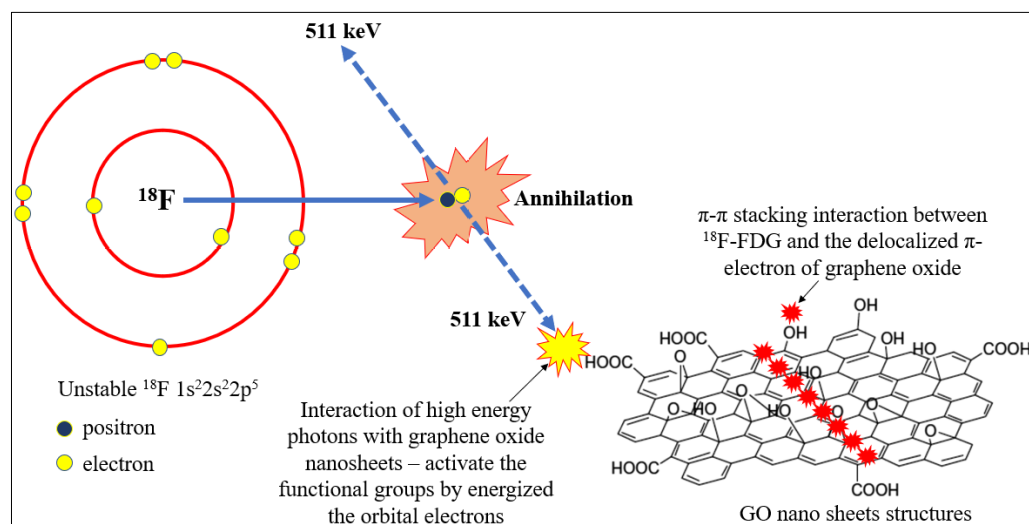


**Figure 12.** Illustration of energetic gamma rays produced by unstable  $^{18}\text{F}$  when activating the adsorption process with functional groups and GO nanosheet structures.

#### 4. Conclusions

Conclusively, GO has demonstrated high sorption affinity towards the radionuclide of a pure radiopharmaceutical. The high sorption capacity and the ability to coagulate with any reactive elements at molecular structures, such as  $^{18}\text{F}$ -FDG, makes it a prime option for alternative radionuclides decontamination. The ‘wax tissue’ nanolayers and vast surface area have been shown to help GO wrap and adsorb radionuclides effectively. The adsorption rate was effective at a slow decay rate of  $^{18}\text{F}$ -FDG, where more available free



electrons are ready for the adsorption interaction with GO functional groups. Fluctuation of electron interactions and the active annihilation process occurred at high activity, thereby reducing the coagulation process within a short time due to the energetic nuclear process. The optical adsorption of GO with  $^{18}\text{F}$ -FDG is dominated by the  $\pi \rightarrow \pi^*$  plasmon peak, which is near 230 nm.

**Author Contributions:** Conceptualization, M.K.A.A.R. and A.M.N.; methodology, M.K.A.A.R., A.M.N. and N.H.A.; software, N.H.A. and F.A.M.Z.; validation, M.K.A.A.R., A.M.N. and N.H.A.; formal analysis, M.K.A.A.R., F.H.M.H., A.M.N. and F.A.M.Z.; investigation, M.K.A.A.R., N.M.N.; resources, M.K.A.A.R., N.M.N., A.M.N., M.M. and F.A.M.Z.; data curation, F.H.M.H., R.S. and F.I.; writing—original draft preparation, M.K.A.A.R. and F.H.M.H.; writing—review and editing, M.K.A.A.R., N.M.N., A.M.N.; visualization, M.K.A.A.R., A.M.N.; supervision, M.K.A.A.R., N.M.N., N.H.A. and M.M.; project administration, F.H.M.H., R.S. and F.I., M.M.; funding acquisition, M.K.A.A.R. and N.M.N. All authors have read and agreed to the published version of the manuscript.

**Funding:** This work was supported by a Short-Term Research Grant from Universiti Sains Malaysia [304/PPSK/6315499]. The APC was funded by Universiti Sains Malaysia.

**Institutional Review Board Statement:** Not applicable.

**Informed Consent Statement:** Not applicable.

**Data Availability Statement:** Not applicable.

**Acknowledgments:** We express our appreciation to Nik Fakurudin Nik Ali and Wan Norhasikin Wan Marizam of the School of Health Sciences, Universiti Sains Malaysia, for their help in obtaining the FESEM micrographs. Our appreciation goes to the Department of Nuclear Medicine, Radiotherapy & Oncology, Hospital Universiti Sains Malaysia and Nuclear Medicine & Molecular Imaging Department, Chancellor Tuanku Muhriz Hospital, Universiti Kebangsaan Malaysia for the use of their facilities when conducting the research project.

**Conflicts of Interest:** The authors declare no conflict of interest.

## References

1. Payolla, B.; Massabni, A.F.; Orvig, C. Radiopharmaceuticals for Diagnosis in Nuclear Medicine: A short review. *Eclat. Quim.* **2019**, *44*, 11–19. [\[CrossRef\]](#)
2. Jacobson, O.; Kiesewetter, D.; Chen, X. Fluorine-18 Radiochemistry, Labeling Strategies and Synthetic Routes. *Bioconjugate Chem.* **2014**, *26*, 1–18. [\[CrossRef\]](#) [\[PubMed\]](#)
3. Park, B.; Kitteringham, N. Effects of Fluorine Substitution on Drug Metabolism: Pharmacological and Toxicological Implications. *Drug Metab. Rev.* **1994**, *26*, 605–643. [\[CrossRef\]](#) [\[PubMed\]](#)
4. Nawi, N.M.; Ahmad, N.S.; Abdullah, R.; Zainon, W.M.N.W.; Razab, M.K.A.A. Correlation of external dose rate with whole body clearance estimation in radioiodine therapy for rhTSH and THW patients. *J. Radiat. Res. Appl. Sci.* **2020**, *13*, 240–245. [\[CrossRef\]](#)
5. Ramesha, G.; Vijaya Kumara, A.; Muralidhara, H.; Sampath, S. Graphene and graphene oxide as effective adsorbents toward anionic and cationic dyes. *J. Colloid Interface Sci.* **2011**, *361*, 270–277. [\[CrossRef\]](#)
6. Jiang, W.; Chalich, Y.; Deen, M.J. Sensors for Positron Emission Tomography Applications. *Sensors* **2019**, *19*, 5019. [\[CrossRef\]](#)
7. Shivanand, B.; Akchata, S.; Lavanya, K. Influence of decontaminating agents and swipe materials on laboratory simulated working surfaces wet spilled with sodium pertechnetate. *Indian J. Nucl. Med.* **2017**, *32*, 173–176. [\[CrossRef\]](#)
8. Lee, W.; Ojovan, M.; Jantzen, C. *Radioactive Waste Management and Contaminated Site Clean-Up*; Woodhead Publishing: Cambridge, UK, 2013; pp. 301–326.
9. Fu, S.; Sun, Z.; Huang, P.; Li, Y.; Hu, N. Some Basic Aspects of Polymer Nanocomposites: A critical review. *Nano Mater. Sci.* **2019**, *1*, 2–30. [\[CrossRef\]](#)
10. Smith, A.; LaChance, A.; Zeng, S.; Liu, B.; Sun, L. Synthesis, properties, and applications of graphene oxide/reduced graphene oxide and their nanocomposites. *Nano Mater. Sci.* **2019**, *1*, 31–47. [\[CrossRef\]](#)
11. Sajjad, S.; Leghari, S.A.K.; Iqbal, A. Study of Graphene Oxide Structural Features for Catalytic, Antibacterial, Gas Sensing and Metals Decontamination Environmental Applications. *ACS Appl. Mater. Interfaces* **2017**, *9*, 43393–43414. [\[CrossRef\]](#)
12. Zhao, Y.; Zhang, Z.; Pan, Z.; Liu, Y. Advanced Bioactive Nanomaterials for Biomedical Applications. *Exploration* **2021**, *1*, 20210089. [\[CrossRef\]](#)
13. Novacek, M.; Jankovsky, O.; Luxa, J.; Sedmidubsky, D.; Pumera, M.; Fila, V.; Lhotka, M.; Klimova, K.; Matejkova, S.; Sofer, Z. Tuning of Graphene Oxide Composition by Multiple Oxidations for Carbon Dioxide Storage and Capture of Toxic Metals. *J. Mater. Chem. A* **2017**, *5*, 2739–2748. [\[CrossRef\]](#)

14. Prasad, S.; Suresh, S.; Wong, R. Osteogenic Potential of Graphene in Bone Tissue Engineering Scaffolds. *Materials* **2018**, *11*, 1430. [\[CrossRef\]](#)
15. Raccichini, R.; Varzi, A.; Passerini, S.; Scrosati, B. The Role of Graphene for Electrochemical Energy Storage. *Nat. Mater.* **2015**, *14*, 271–279. [\[CrossRef\]](#) [\[PubMed\]](#)
16. Ng, Y.H.; Ikeda, S.; Matsumura, M.; Amal, R. A Perspective on Fabricating Carbon-based Nanomaterials by Photocatalysis and their Applications. *Energy Environ. Sci.* **2012**, *5*, 9307–9318. [\[CrossRef\]](#)
17. Wen, J.; Xu, Y.; Li, H.; Lu, A.; Sun, S. Recent Applications of Carbon Nanomaterials in Fluorescence Biosensing and Bioimaging. *Chem. Commun.* **2015**, *51*, 11346–11358. [\[CrossRef\]](#)
18. Shtein, M.; Nadiv, R.; Buzaglo, M.; Kahil, K.; Regev, O. Thermally Conductive Graphene Polymer Composites: Size, Percolation and Synergy Effects. *Chem. Mater.* **2015**, *27*, 2100–2106. [\[CrossRef\]](#)
19. Zunita, M.; Irawanti, R.; Koesmawati, T.A.; Lugitoa, G.; Wenten, I.G. Graphene Oxide (GO) Membrane in Removing Heavy Metals from Wastewater: A Review. *Chem. Eng. Trans.* **2020**, *82*, 415–420.
20. Ng, L.Y.; Chua, H.Y.; Ng, C.Y. Incorporation of Graphene Oxide-based Nanocomposite in the Polymeric Membrane for Water and Wastewater Treatment: A review on Recent Development. *J. Environ. Chem. Eng.* **2021**, *9*, 105994. [\[CrossRef\]](#)
21. Aunkor, M.T.H.; Raihan, T.; Prodhan, S.H.; Metselaar, H.S.C.; Malik, S.U.F.; Azad, A.K. Antibacterial Activity of Graphene Oxide Nanosheet Against Multidrug Resistant Superbugs Isolated from Infected Patients. *R. Soc. Open Sci.* **2020**, *7*, 200640. [\[CrossRef\]](#)
22. Eigler, S.; Hirsch, A. Chemistry with Graphene and Graphene Oxide—Challenges for Synthetic Chemists. *Angew. Chem. Int. Ed.* **2014**, *53*, 7720–7738. [\[CrossRef\]](#) [\[PubMed\]](#)
23. Sabzehmeidani, M.M.; Mahnaee, S.; Ghaedi, M.; Heidari, H.; Roy, V.A.L. Carbon Based Materials: A review of Adsorbents for Inorganic and Organic Compounds. *Mater. Adv.* **2021**, *2*, 598–627. [\[CrossRef\]](#)
24. Felton, E. *Technology Reference Guide for Radiologically Contaminated Surfaces*; U.S. Environmental Protection Agency: Washington, DC, USA, 2006; pp. 11–18.
25. Zhao, G.; Wen, T.; Yang, X.; Yang, S.; Liao, L.; Hu, J.; Shao, D.; Wang, X. Preconcentration of U(VI) Ions on Few-layered Graphene Oxide Nanosheets from Aqueous Solutions. *Dalton Trans.* **2012**, *41*, 6182–6188. [\[CrossRef\]](#)
26. Rauwel, P.; Rauwel, E. Towards the Extraction of Radioactive Cesium-137 from Water via Graphene/CNT and Nanostructured Prussian Blue Hybrid Nanocomposites: A Review. *Nanomaterials* **2019**, *9*, 682. [\[CrossRef\]](#) [\[PubMed\]](#)
27. Suksompong, T.; Thongmee, S.; Sudprasert, W. Efficacy of a Graphene Oxide/Chitosan Sponge for Removal of Radioactive Iodine-131 from Aqueous Solutions. *Life* **2021**, *11*, 721. [\[CrossRef\]](#) [\[PubMed\]](#)
28. Romanchuk, A.Y.; Slesarev, A.S.; Kalmykov, S.N.; Kosynkin, D.V.; Tour, T.M. Graphene Oxide for Effective Radionuclide Removal. *Phys. Chem. Chem. Phys.* **2013**, *15*, 2321–2327. [\[CrossRef\]](#)
29. Noor, A.M.; Yusoff, N.F.A.; Huang, N.M.; Kari, Z.A.; Razab, M.K.A.A.; Bakar, M.H.A.; Lee, S.W.; Abdullah, N.H. Facile Preparation of Graphene Oxide Silver Aerogel for Antibacterial. *J. Trop. Resour. Sustain. Sci.* **2018**, *6*, 41–44.
30. Zin FA, M.; Noor, A.M.; Razab, M.K.A.A.; Abdullah, N.H.; Lee, S.W. Synthesis of Silver Graphene Oxide Nanocomposite Reinforced with Kenaf Cellulose Nanofibril Aerogel. *AIP Conf. Proc.* **2019**, *2068*, 020045-1–020045-6.
31. Noor, A.M.; Zin, F.M.; Wei, L.S.; Huang, N.M.; Bakar, M.H.A.; Sajab, M.S.; Razab, M.K.A.A.; Abdullah, N.H.; Kari, Z.A. Laser Scribe Silver-reduced Graphene Oxide as Novel Bactericidal Filter. *AIP Conf. Proc.* **2019**, *2068*, 020026-1–020026-6.
32. Zobir, S.A.M.; Rashid, S.A.; Tan, T. Recent Development on the Synthesis Techniques and Properties of Graphene Derivatives. In *Synthesis, Technology and Applications of Carbon Nanomaterials*; Rashid, S.A., Othman, R.N.I.R., Hussein, M.Z., Eds.; Matthew Deans: Oxford, UK, 2019; pp. 77–107.
33. Razab, M.K.A.A.; Mansor, M.S.; Noor, A.M.; Latif, N.F.F.A.; Rozi, S.M.; Jaafar, K.N.; Jamaludin, F. Characterization of GO:I-131 for Radioactive Clinical Waste Water Management in Nuclear Medicine. *Mater. Sci. Forum.* **2020**, *1010*, 561–566. [\[CrossRef\]](#)
34. Razab, M.K.A.A.; Mansor, M.S.; Noor, A.M.; Rozi, S.M.; Latif, N.F.F.A.; Jaafar, K.N.; Jamaludin, F. Preliminary Study of the Potential Graphene Oxide as Radioactive Clinical Wastewater Adsorbability in Nuclear Medicine. *IOP Conf. Ser. Earth Environ. Sci.* **2020**, *96*, 012037. [\[CrossRef\]](#)
35. Díez-Pascual, A.; Sainz-Urruela, C.; Vallés, C.; Vera-López, S.; San Andrés, M. Tailorable Synthesis of Highly Oxidized Graphene Oxides via an Environmentally-Friendly Electrochemical Process. *Nanomaterials* **2020**, *10*, 239. [\[CrossRef\]](#) [\[PubMed\]](#)
36. Yang, N.; Yang, D.; Zhang, G.; Chen, L.; Liu, D.; Cai, M.; Fan, X. The Effects of Graphene Stacking on the Performance of Methane Sensor: A First-Principles Study on the Adsorption, Band Gap and Doping of Graphene. *Sensors* **2018**, *18*, 422. [\[CrossRef\]](#) [\[PubMed\]](#)
37. Kamali, N.; Ghasemi, J.B.; Ziarani, G.M.; Moradian, S.; Badiei, A. Design, Synthesis, and Nanoengineered Modification of Spherical Graphene Surface by LDH for Removal of As(III) from Aqueous Solutions. *Chin. J. Chem. Eng.* **2022**, in press. [\[CrossRef\]](#)
38. Aliyev EFiliz, V.; Khan, M.M.; Lee, Y.J.; Abetz, C.; Abetz, V. Structural Characterization of Graphene Oxide: Surface Functional Groups and Fractionated Oxidative Debris. *Nanomaterials* **2019**, *9*, 1180. [\[CrossRef\]](#)
39. Smajlagic, I.; Rowshanpour, R.; Milkin, L.; Dudding, T. Organofluorine Compounds in Fluorine-18 Positron Emission Tomography Imaging. *Res. Rev. Health Care Open Acc. J.* **2020**, *5*, 488–491.
40. Kuilla, T.; Bhadra, S.; Yao, D.; Kim, N.H.; Bose, S.; Lee, J.H. Recent Advances in Graphene Based Polymer Composites. *Prog. Polym. Sci.* **2010**, *35*, 1350–1375. [\[CrossRef\]](#)
41. Jenkins, D. Nuclear Structure and Radioactive Decay. In *Radiation Detection for Nuclear Physics*; IOP Publishing: Bristol, UK, 2020; pp. 1–32.

42. Alauddin, M.M. Positron Emission Tomography (PET) Imaging with  $^{18}\text{F}$ -based Radiotracers. *Am. J. Nucl. Med. Mol. Imaging* **2012**, *2*, 55–76.
43. Yang, S.; Chen, Q.; Shi, M.; Zhang, Q.; Lan, S.; Maimaiti, T.; Li, Q.; Ouyang, P.; Tang, K.; Yang, S.T. Fast Identification and Quantification of Graphene Oxide in Aqueous Environment by Raman Spectroscopy. *Nanomaterials* **2020**, *10*, 770. [[CrossRef](#)]
44. Zin, F.A.M.; Noor, A.M.; Lee, S.W.; Sajab, M.S.; Razab, M.K.A.A.; Abdullah, N.H.; Ishak, W.M.F.W.; Wong, K.N.S.S.; Zaudin, N.A.C. Graphene Oxide Silver Cellulose Alginate for Antibacterial. *Mater. Sci. Forum.* **2020**, *1010*, 590–595.
45. Maslekar, N.; Zetterlund, P.B.; Kumar, P.V.; Agarwal, V. Mechanistic Aspects of the Functionalization of Graphene Oxide with Ethylene Diamine: Implications for Energy Storage Applications. *ACS Appl. Nano Mater.* **2021**, *4*, 3232–3240. [[CrossRef](#)]
46. Lai, Q.; Zhu, S.; Luo, X.; Zou, M.; Huang, S. Ultraviolet-visible Spectroscopy of Graphene Oxides. *AIP Adv.* **2012**, *2*, 032146-1–032146-5. [[CrossRef](#)]
47. Yu, L.; Yan, Q.; Ruzsinszky, A. Key Role of Antibonding Electron Transfer in Bonding on Solid Surfaces. *Phys. Rev. Mater.* **2019**, *3*, 092801. [[CrossRef](#)]